Nanoscale

Accepted Manuscript

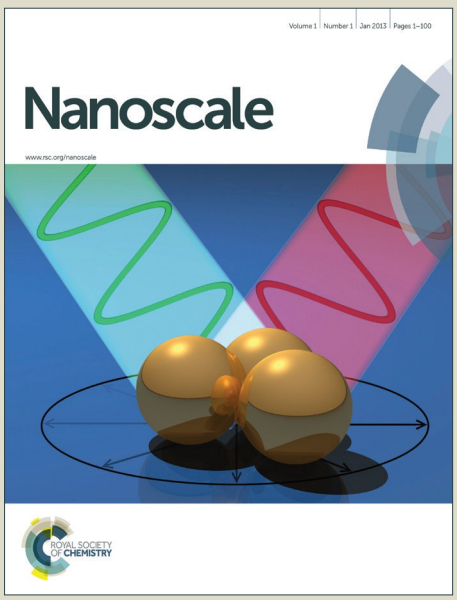

ROYAL SOCIETY OF CHEMISTRY

www.rsc.org/nanoscale

Nanoscale

RSCPublishing

ARTICLE

Reprocessable Squeezing Electrode Fabrication of Olive-Like Fe/Co/O Nanoparticles@Three Dimensional Nitrogen-doped Reduced Graphene Oxide for High Performance Lithium Battery

Cite this: DOI: 10.1039/x0xx00000x

Received 00th January 2012,
Accepted 00th January 2012

DOI: 10.1039/x0xx00000x

www.rsc.org/

Li-Ya Qi,[a] Yi-Wei Zhang,[a] Yue-Long Xin,[a] Zi-Cheng Zuo,[b] Bin Wu,[b*] Xin-Xiang Zhang[a] and Heng-Hui Zhou[a*]

Abstract: A one step in-situ synthesis approach is developed to construct 3D nitrogen-doped reduced graphene oxides, in which the olive-like multi-component metal oxides are homogeneously dispersed. The novel hybrid nanoarchitecture can create some particular properties from synergistic effects. The size of Fe/Co/O oxides is reduced and better controlled compared to that of individuals due to mutual dispersant interaction. Furthermore, the positive synergistic interaction between heterogeneous oxides and graphene nanosheets has an effective control on the particle size and dispersion of nanoparticles. Taking advantage of the flexibility and the cohesiveness of graphene nanosheets, the obtained composite can be directly processed into a binder-free electrode through a unique time-saving "squeezing" process. The obtained electrode possesses a reprocessable feature, which provides possibilities for convenient-storage and quick-fabrication at any time and presents attractive electrochemical performance of robust long-term capability retention (562 mA h g^{-1} after 300 cycles at 10A g^{-1}) and superior rate performances (1162 mA h g^{-1} at 0.5 A g^{-1}, 737 mA h g^{-1} at 5 A g^{-1}, and 585 mA h g^{-1} at 10 A g^{-1}).

1 Introduction

Constructing hybrid nanocomposites[1-4] especially transition metal oxide (TMO, M = Fe, Co, Ni, or Mn)-graphene anodes[5-7] are extensively investigated for the development of next generation Li ion batteries (LIBs) owing to the ever-growing energy needs. Graphene with its large specific surface area and excellent electrical conductivity can accommodate mechanical strain caused by volume expansion of TMOs.[8-10] Through optimizing particle size, it forms short pathways for the electrons and ions which guarantees high transport rate and large electrode/electrolyte contact area.[11-14] Hybrid nanocomposites can usually create some particular properties from synergistic effects. For example, in a heterogeneous oxide growth system, each oxide can play the role as mutual dispersants, thus not only impeding the growth but controlling aggregating to some extent during electrochemical reactions.[15, 16] Furthermore, the synergistic interaction between heterogeneous oxides and graphene nanosheets (GS) is believed to have a positive effect on controlling the size and dispersion of nanoparticles.[17-19]

Most of the reported graphene-based hybrid electrodes are made through a "slurry-casting" method, which requires mixing active materials with binders and conductive carbon additives. However, the prevailing chemically exfoliated graphene oxide (GO)[20, 21] followed with post-reduction lead to an inhomogeneous mixture due to the poor dispersity of GS, thus influencing the diffusion paths of ions and electrons in the electrode.[22, 23] The additives that hardly contribute to capacitance, however, significantly affect the overall electrochemical performance[23-25] which reduce the electron conductivity and energy density. Recently, there are several reports that have shown the free-standing paper like carbon-based materials, owned with light weight and high conductivity, are promising for high energy density electrodes and can avoid electric disconnection between active materials and current collectors due to the volume change.[26-28] However, most of methods referred are focused on vacuum filtration or chemical vapor deposition (CVD), in which either surfactants are usually necessary or complex preparation

and/or expensive experimental facilities are needed. There are a few reports about some novel and easy fabrication. Liu et al. made graphene papers by mechanically pressing a graphene aerogel[29] and Yin et al. developed a scalable self-assembly method to create hierarchical structures made of functionalized GS.[30] But these strategies are mainly concentrated on preparing pure graphene papers. Seeking for new and simple preparation method to construct hybrid materials with some specific properties from synergistic effects are worth exploring. To the best of our knowledge, little research has mentioned the method to process graphene nanocomposites into large-scale binder-free Li-ion anode electrodes exhibiting a "reprocessable" feature. It is imperative to realize low-cost production electrodes through a rapid and broadly applicable fabrication.

In this article, we designed a time-saving and economical "squeezing" method to make electrodes. First, a facile approach was employed to construct 3D N-doped reduced graphene oxide embedded with olive-like multi-component metal oxides (Fe/Co/O@3D N-rGO). 3D interconnected frameworks[31-33] will generate multidimensional pathways for both electrons and lithium ions. Besides, by substituting heteroatom of the original graphene,[34-36] it is expected to increase the lithium storage performance and fortify electronic conductivity. The synergetic effects resulting from the 3D construction of nitrogen-doped graphene nanosheets and metal oxides nanoparticles are believed to realize a better utilization of the electrochemically active materials. Furthermore, based on a small amount of residual hydrophilic oxygenated groups which play as a glue in mechanical pressing preparation coupled with the π–π interaction result in successful construction of graphene paper. In the novel reprocessable "squeezing" method, not only are electrodes easy to make, but once grinded into pieces, they are again able to be rolled into electrodes by straightforward squeezing. Benefitting from the above superiorities, the novel free-standing electrodes (Fe/Co/O@3D N-rGO) presents high rate capability (1162 mA h g^{-1} at 0.5 A g^{-1}, 737 mA h g^{-1} at 5 A g^{-1}, and 585 mA h g^{-1} at 10 A g^{-1}) and extremely excellent cycle performances at high rates (upon 300 cycles of maintaining 562 mA h g-1 at a high rate of 10 A g^{-1}).

2 Experimental

2.1 Preparation of Fe/Co/O@ 3D N-rGO:

All chemicals were of analytical grade and directly used without further purification. GO was synthesized from graphite powder by the modified Hummers method. 0.4 mmol of Fe $(NO_3)_3{\cdot}6H_2O$ and 0.6 mmol of $Co(NO_3)_2{\cdot}4H_2O$ were dissolved in 30 ml GO dispersion (1 mg mL^{-1}) to form uniform mixed solution of Fe / Mn molar ratio of 1:1. 200 μL $NH_3{\cdot}H_2O$ was added slowly and followed by ultrasonicating for 30 min. Then 3 g $(NH_4)_2CO_3$ acting as the N source and reducing agent was added. After stirred for 10 min, the resulting uniform suspension was sealed in a 50 mL Teflon-lined autoclave and hydrothermally treated at 180 °C for 12 h. Then the product was washed with distilled water for several times and treated by freeze-drying and heat treatment in a tube furnace at 300 ° C for 3 h under N_2 flow.

Preparation of individual metal oxide@N-rGO: For comparison, individual metal oxide Fe_2O_3 @3D N-rGO and Co_3O_4 @3D N-rGO were also prepared by using the same procedure for Fe/Co/O@ 3D N-rGO.

Preparation of physical mixture Fe/Co/O@3D N-rGO: Fe-Co-O synthesized in advance directly mixed with GO and $(NH_4)_2CO_3$ for 30 min sonication, then using the same procedure as above.

2.2 Morphology and composition Characterizations

Powder X-ray diffraction (XRD, X Pert Pro diffractometer) measurements were tested with Cu−Kα irradiation (λ = 0.15406 nm). Raman spectra (L2BRAM ARAMIS) were recorded with an excitation laser beam wavelength of 532 nm. The X-ray photoelectron spectrum (XPS, Axis Ultra) was conducted by using a Mg−Kα radiation exciting source. Emission scanning electron microscope (SEM, Hitachi S-4800), transmission electron microscope (TEM, Tecnai F20 S-Twin) combined with an energy-dispersive X-ray spectrometer (EDX, Hitachi S-4800) were used to observe the morphology of the sample. Thermo gravimetric analysis (TGA, TA Q5000IR) was measured from ambient temperature to 1000 °C in air at a heating rate of 10 °C min^{-1}. Nitrogen adsorption/desorption isotherms at 77 K were determined by Micromeritics ASAP 2010.

2.3 Electrochemical tests

Electrochemical performances of all the samples were assessed in 2032 type coin cells. Free-standing samples were operated on a roller grinding machine (DG-WZ100, China) by directly squeezing into thinner sheet without other additives. The electrolyte consisted of a solution of 1 M $LiPF_6$ in ethylene carbonate/dimethyl carbonate (EC), diethyl carbonate (DMC) (1:1:1 in weight percent). The discharge and charge cycles were carried on a LAND system in the voltage range of 0.01–3.00 V at various current densities. Cyclic voltammtery (CV, Autlab PGSTAT302N) measurements were obtained in the potential range of 0.0−3.0 V at a scan rate of 0.1mV s^{-1}. Electrochemical impedance spectroscopy (EIS) was tested on the same electrochemical work station.

3 Results and Discussion

Figure 1 illustrates the preparation process for Fe/Co/O@3D N-rGO paper. Through hydrothermal treatment with $(NH_4)_2CO_3$, 2D GO with a uniform decoration of the two metal oxide precursors acted as building blocks and self-assembled into 3D integral networks owing to the decreased oxygenated groups on surface of GN. By simply squeezing the foam-like pieces, the controllable-area paper anodes is obtained. Free-standing electrodes possess the merits of an economic and time-saving manufacturing operation. Notably, as shown in Figure 2, graphene paper was successfully constructed through a mechanical squeezing process owed to the small amount of residual hydrophilic oxygenated groups that acted as a glue and the accompanied π–π interaction. Once grinded into pieces, the paper-like electrode are again able to be rolled into electrodes by straightforward squeezing thus forming a reprocessable cycle. It is the first time that a unique "squeezing" fabrication method is raised up along with reprocessable feature, which provide possibilities for convenient-storage and quick-fabrication at any time.

SEM image (Figure S1a, supporting information) reveals the 3D well dispersed macropore graphene networks. The olive-like morphology of Fe/Co/O particles with uniform dispersion are clearly presented in Figure 3a with 30 nm diameter and length in the range of 80-120 nm. 1D Elongated olive-like nanocrystals are rarely reported before. Clearly, 1D nanomaterials are superior than 0 D nanoparticles surface due to a larger specific area.[37] This fantastic morphology should be attributed to synergistic interactions between nanoparticles and GS. The geometric confinement of graphene layers inhibits the growth of the nanoparticles and furthermore drives the coalescence of two or more nanoparticles into elongated nanostructures that look like the olives (Figure 3b, S1b and 1c,

S2). It confirms the existence of nanoparticles embedded between continuous conductive networks instead of being distinctly exposed on the surface by simply mixing method of Fe/Co/O+3D N-rGO, in which most of the exposed nanoparticles are of severe agglomeration (Figure S3a). It is obvious that the presence of graphene plays an important role in tailoring the crystal growth of Fe/Co/O. The aggregation and volume variation of nanoparticles can be effectively suppressed through such a unique geometric confinement, thus enhancing electrode stability upon cycles. The well-defined lattice fringes of 0.28 and 0.37 nm in different regions are in accord with the (220) and (012) crystalline plane of the Co_3O_4[38] and Fe_2O_3[39] phase respectively (Figure 3c),which correspond to XRD results (Figure 4a).The folded structure of the graphene with fewer layers is presented (Figure 3d and S1d), which can provide more lithium insertion active sites.[29] Energy-dispersive X-ray (EDX) mapping analysis results (Figure S4) further confirm the uniform distribution of the Fe_2O_3 and Co_3O_4. Because of the coexistence of the two metal oxides, we obtain particles of much smaller diameter size compared with any individual growth of Fe_2O_3 or Co_3O_4 in Figure S3b and S3c, though both of the samples are well-dispersed within thin GS.

The XRD patterns of the products by calcination after 300 °C in N_2 are shown in Figure 4a. All the diffraction peaks correspond to those for Fe_2O_3 (JCPDS card No. 33-0664)[39] and Co_3O_4 (JCPDS card No. 42-1467)[40], which prove that the Fe/Co/O@3D N-rGO composites have no other impurity phase. No apparent diffraction peak in the range of 24–28° are observed which suggests only a slightly stacking of GS.[17] BET analysis of nitrogen adsorption / desorption isotherms reveals that the specific surface area of Fe/Co/O@3D N-rGO is as high as 100.5 m^2 g^{-1}(Figure 4b), which is much larger than bare metal oxides. Moreover, an average 7.2 nm mesopore (the inset in Figure 4b) is obtained based on the Barrett–Joyner–Halenda model. This result convinces it that through our facile hydrothermal treatment, it is effective to build up 3D frameworks with meso- and macro-porous features of high surface area. Not merely can it facilitate better diffusion and accession of electrolyte ions through pore channels but also alleviate the volume expansion due to the buffer space of this structure. From this viewpoint, excellent electrochemical performance is predictable for the Fe/Co/O@3D N-rGO composite paper. TGA (Figure S5a) result carried out in the air indicates the chemical content of the Fe/Co/O@3D N-rGO. According to the remaining weight, the original fraction of metal oxides is calculated to be 68.7%.

Based on the images of XPS (Figure 4c and 4d), our method is proved to be an effective strategy to synthesize N-doped graphene. The prevailing synthetic approaches of N-doped graphene such as CVD,[41, 42] hydrothermal reduction by hydrazine hydrate[18] and thermal annealing of GO with NH_3[34] result in complex operations and the precursors are usually corrosive and toxic. Herein, we turned 2D GO into well-organized 3D N-GF structure with high N doping level by an environment-friendly hydrothermal settlement in virtue of in-situ producing ammonia by decomposition of $(NH_4)_2CO_3$. The N1s peaks centered at 398.5, 399.9, and 402.0 eV stand for pyridinic, pyrrolic and graphitic type of N atoms doped in the graphene structure,[19] respectively. Moreover, the atomic percentage of doped nitrogen is about 7.56%, which is comparable to that obtained by using a traditional ammonia-mediated CVD method.[42] The main peak of the C1s core-level spectrum at 284.7 eV is assigned to sp^2 hybridized C atoms in graphene, whereas the other two peaks at 285.6, 288.3 and 291.9 eV are fitted with sp^2 C and sp^3 C atoms bonded to N, respectively.[19, 41] The shift ratio of D (1339 cm^{-1}) and G bands (1594 cm^{-1}) in Raman spectra (Figure S5b) from 0.86 to 1.04 for GO and Fe/Co/O@3D N-rGO, respectively manifests that the doped graphene is more disordered than the pristine one[35]. As studies showed,[35, 36] the suitable defects derived from N-rGO provide more active sites for electron storage and the diffusion barriers are greatly lowered, further expediting the Li^+ diffusion across the graphene layers.

Figure S6a depicts the representative CVs of Fe/Co/O@3D N-rGO for the first three cycles between 0.0 - 3.0 V at a scan rate of 0.1 mV/s. When the electrodes are scanned cathodically for the first cycle curve, a well-defined peak at 0.56 V corresponds to the reduction of Fe_2O_3 to Fe[13] and Co_3O_4 to Co.[43] The additional peak at 1.56 V is attributed to the multistep electrochemical lithium reduction for Co_3O_4 on account of the complex redox reaction of Co^{n+}/Co (n is between 2 and 3).[43] The anodic peak at 1.75 V is attributed to the reversible oxidation of Co and Fe to Co_3O_4 and Fe_2O_3. Obviously, the first CV curve cycle is quite different from the subsequent ones mainly due to the solid electrolyte interphase (SEI) formation and the decomposition of the electrolyte on the surface of the nanosized particles.[44] From the second cycle, the main distinct peak appeared around 1.86 V for the anodic process and 0.79 V for the cathodic process are ascribed to the concurrent reactions for Co_3O_4 and Fe_2O_3. This further confirmed the composite effect of the two oxides. Moreover, the intensity and shape of the third cycle curve resemble that of the second one. These results indicate a stable SEI film and GN can prevent the direct contact of encapsulated Fe/Co/O nanoparticles with electrolyte, thus keeping the structural integrity during subsequent cycles. In conclusion, the reversible reaction occurring with lithium in the sample can be described as follows: $Fe_2O_3 + Co_3O_4 + 14\ Li + 14\ e^- \leftrightarrow 2\ Fe + 3\ Co + 7\ Li_2O$. The voltage/capacity correlative plateau regions observed in the initial three charge / discharge cycles was in good agreement with CV profiles (Figure S6b). The first discharge and charge capacities are 1943 and 1207 mA h g^{-1} (the value of capacity is based on the total mass of the Fe/Co/O@3D N-rGO) with initial coulombic efficiency of 62.1 %. The capacity loss is mainly ascribed to the formation of SEI layer.[6, 45] In the following cycles, the capacity of 1162 mA h g^{-1} is obtained at a current density of 500 mA g^{-1}, more than a 3-fold increase compared to graphite (372 mA h g^{-1}). Such high capacities should owe to positive synergistic interaction of heteroatomic graphene and Fe/Co/O nanoparticles as mentioned above.

As revealed in Figure 5a, it exhibits the comparison of rate performance of three samples at different current densities of 500, 1000, 2000, 3000, 4000, 5000, 10000 mA g^{-1}, respectively. For Fe/Co/O@3D N-rGO, even at very high current densities such as 5000 and 10000 mA g^{-1}, reversible capacities are retained of 737 and 585 mA h g^{-1} which both exceed the capacity of graphite at low current densities (372 mA h g^{-1}). In the subsequent cycles, the coulombic efficiency reaches nearly 100 %, indicating an efficient transport of ions and electrons in the electrode. When the current density returns to 500 mA g^{-1}, a capacity of 1147 mA h g^{-1} is recovered in another 5 cycles. The poorer rate performances of Fe_2O_3@3D N-rGO and Fe/Co/O+3D N-rGO are attributed to the larger crystallites and severe agglomeration because short pathways for the electrons and ions guarantee high transport rate. For comparison, we also presented the result of rGO evaluated by charge/discharge cycling at different current densities (Figure S7). Apparently, the rate capability of our Fe/Co/O@3D N-rGO are superior to

most of the previous reported graphene-based hybrids (few of them have reported the rate performance above 5000 mA g^{-1} current density). The comparative cycle performance (Figure 5c) was tested at a current density of 1000, 3000, 7000 mA g^{-1} which showed remarkable lithium capacity retention for Fe/Co/O@3D N-rGO. After 500 cycles, the capacity still remains at 1058, 797, 606 mA h g^{-1}, respectively and columbic efficiency is nearly 100 % per cycle after the first one. Even at a high current density of 10000 mA g^{-1} (Figure 5d), the capacity reaches as high as 562 mA h g^{-1} after 300 cycles, maintaining 94.4 % of the initial capacity. They are much higher than those of Fe_2O_3@3D N-rGO (76 mA h g^{-1} after 300th cycle) prepared under the same conditions, which suggests the advantages of the composite oxides over the individuals in cycle performance. In case of Fe/Co/O+3D N-rGO, their capacity rapidly decays from 98 to 31 mA h g^{-1}. Herein, our work demonstrates one of the best cycle performances in terms of high rate in the reported literature. Electrochemical impedance spectroscopy (EIS) was also performed for the three sample of Fe/Co/O@3D N-rGO, Fe_2O_3@3D N-rGO and Fe/Co/O+3D N-rGO (Figure S8a). The experimental Nyquist plots were modeled by an equivalent circuit model based on the EIS results (Figure S8b) and the fitted impedance parameters were summarized in Table S1. The intercept of the high-frequency semicircle can be attributed to the resistance of electrolyte (Re), the resistance of the surface film formed on the electrodes (R_{SEI}) and charge−transfer resistance (Rct). The slope line at low frequency is related to Warburg impedance (Zw), corresponding to the diffusion of lithium ions into the bulk electrode. As shown, the values of SEI film resistance R_{SEI} and charge−transfer resistance R_{ct} of the sample electrode are 27.9 and 30.7, which were significantly lower than those of Fe_2O_3@3D N-rGO and Fe/Co/O+3D N-rGO (78.4 and 159.2, 149.8 and 581.9, respectively). It is convinced that the unique architecture can not only improves the high conductivity of the overall electrode but also largely enhances the electrochemical activity.

To verify the structural integrity, Fe/Co/O@3D N-rGO sample was disassembled and examined by SEM after severe volume expansion / contraction upon long cycles at 1000 mA g^{-1}. As shown in Figure S9, the Fe_2O_3 and Co_3O_4 particles were still of good dispersion and well-confined within buffer matrix, but grew slightly because of the formation of SEI layer. The primary morphology is well maintained due to the ability of robust structure undergo three-dimensional expansion, which alleviates the mechanical stress and avoid cracking and disintegration of the sample. This further confirms that the novel structures are ideal candidates for the next generation of high performance LIBs.

Equipped with the following unique features, the Fe/Co/O@3D N-rGO paper presents such superior electrochemical performances. First of all, from a practical point of view, the time-saving "squeezing" method to make electrodes is highlighted. Not only are the light mass maintained, which guarantees high energy storage density, but also it avoids the electric disconnection between the active material and the current collector due to the volume change. Moreover, the time-saving manufacture operation possesses a reprocessable feature. Secondly, the synergetic effects resulting from the 3D construction of nitrogen-doped graphene nanosheets and metal oxides fillers realize the maximum utilization of the electrochemically active materials. The covering of elastic GS on the active nanoparticles in our 3D N-rGO structure efficiently buffer the volume changes and prevent the aggregation as well as cracking and crumbling(Figure 6a), which well explain the much better long cycle performance, in contrast with the situation presented in Figure 6b. In case of the simply physical mixture, the exposed nanoparticles after lithiation tend to cluster with each other, much easier to fall off the surface of the graphene, thus leading to fast capacity loss. From the obvious comparison of the transport length (*Le*), our Fe/Co/O@3D N-rGO paper is effectively shortened to a comparable particle size level. Thirdly, inspired by the impeditive growth effect of two different materials, we obtain Fe/Co/O particles of smaller size compared with the individual ones. Due to the high rate and cycle performance highly depend on the rapid ionic and electronic diffusion and transport, the small size of nanoparticles in our case can significantly shorten the lithium ion and electron diffusion distance. Finally, the N-doped graphene favors a larger reversible capacity over pristine graphene and the conductive GS with 3D framework can serve as multidimensional pathways to facilitate the transport of electrons.

Conclusions

In summary, the unique Fe/Co/O@3D N-rGO without any other additives was fabricated through an in-situ synthesis approach. The high capacity, stable cycle stability and excellent rate capability of Fe/Co/O@N-rGO result from the synergistic interactions between Fe_2O_3 and Co_3O_4 particles as well as Fe/Co/O filler nanoparticles and n-doped 3D framework graphene. Moreover, considering the practical usage, the free-standing electrode possesses energy storage density and convenient manufacture operation. The facile strategy can also be extended to build a variety of other interesting multicomponent oxides-graphene hybrid materials for important applications in high-performance LIBs, supercapacitors and catalyst in many scientific fields.

Acknowledgements

A* Star Singapore-China Joint Research program (No. 2012DFG52130)， Technology Innovation Project of New Energy Vehicles Industry and Pulead Technology Industry Co. Ltd are gratefully acknowledged for their financial support for this work.

References

[a] College of Chemistry and Molecular Engineering, Peking University, Beijing, P. R. China.
[b] Beijing Engineering Research Center of Power Lithium-ion Battery, Beijing 102200
*Corresponding author:
E-mail: hhzhou@pku.edu.cn; wubin@pulead.com.cn.
Fax & Tel: +861062757908

† Electronic Supplementary Information (ESI) available. See DOI: 10.1039/b000000x/

1. A. L. M. Reddy, S. R. Gowda, M. M. Shaijumon and P. M. Ajayan, *Adv. Mater.*, 2012, **24**, 5045-5064.
2. P. L. Taberna, S. Mitra, P. Poizot, P. Simon and J. M. Tarascon, *Nat. Mater.*, 2006, **5**, 567-573.
3. R. Liu and S. B. Lee, *J. Am. Chem. Soc.*, 2008, **130**, 2942-2943.
4. L. J. Zhi, Y. S. Hu, B. E. Hamaoui, X. Wang, I. Lieberwirth, U. Kolb, J. Maier and K. Müllen, *Adv. Mater.*, 2008, **20**, 1727-1731.

5. W. D. Zhang, W. Wan, H. H. Zhou, J. T. Chen, X. Y. Wang and X. Z. Zhang, *J. Power Sources*, 2013, **223**, 119-124.
6. Z. S. Wu, W. C. Ren, L. Wen, L. B. Gao, J. P. Zhao, Z. P. Chen, G. M. Zhou, F. Li and H. M. Cheng, *ACS Nano*, 2010, **4**, 3187-3194.
7. W. W. Sun and Y. Wang, *Nanoscale*, 2014, **6**, 11528-11552.
8. L. L. Liu, Z. Q. Niu, L. Zhang and X. D. Chen, *Small*, 2014, **10**, 2200-2214.
9. X. Cui, C. Z. Zhang, R. Hao and Y. L. Hou, *Nanoscale*, 2011, **3**, 2118-2126.
10. S. B. Yang, X. L. Feng, L. Wang, K. Tang, J. Maier and K. Müllen, *Angew. Chem. Int. Ed.*, 2010, **49**, 4795-4799.
11. Y. G. Wang, H. Q. Li, P. He, E. Hosono and H. S. Zhou, *Nanoscale*, 2010, **2**, 1294.
12. Y. G. Guo, J. S. Hu and L. J. Wan, *Adv. Mater.*, 2008, **20**, 2878-2887.
13. B. Wang, J. S. Chen, H. B. Wu, Z. Wang and X. W. Lou, *J. Am. Chem. Soc.*, 2011, **133**, 17146-17148.
14. C. Kang, I. Lahiri, R. Baskaran, W.-G. Kim, Y.-K. Sun and W. Choi, *J. Power Sources*, 2012, **219**, 364-370.
15. T. Li, Y. Y. Wang, R. Tang, Y. X. Qi, N. Lun, Y. J. Bai and R. H. Fan, *ACS Appl. Mater. Interfaces*, 2013, **5**, 9470-9477.
16. M. X. Li, Y. X. Yin, C. J. Li, F. Z. Zhang, L. J. Wan, S. L. Xu and D. G. Evans, *Chem. Comm.*, 2012, **48**, 410-412.
17. W. Wei, S. B. Yang, H. X. Zhou, I. Lieberwirth, X. L. Feng and K. Mullen, *Adv. Mater.*, 2013, 2909-2914.
18. X. Zhou, L. J. Wan and Y. G. Guo, *Adv. Mater.*, 2013, **25**, 2152-2157.
19. X. Wang, X. Q. Cao, L. Bourgeois, H. Guan, S. M. Chen, Y. T. Zhong, D.-M. Tang, H. Q. Li, T. Y. Zhai, L. Li, Y. Bando and D. Golberg, *Adv. Funct. Mater*, 2012, **22**, 2682-2690.
20. W. S. Hummers and R. E. Offeman, *J. Am. Chem. Soc.*, 1958, **80**, 1339-1339.
21. Y. X. Xu, H. Bai, G. W. Lu, C. Li and G. Q. Shi, *J. Am. Chem. Soc.*, 2008, **130**, 5856-5857.
22. D. H. Ha, M. A. Islam and R. D. Robinson, *Nano Lett.*, 2012, **12**, 5122-5130.
23. Y. X. Tang, Y. Y. Zhang, J. Y. Deng, D. P. Qi, W. R. Leow, J. Q. Wei, S. Y. Yin, Z. L. Dong, R. Yazami, Z. Chen and X. D. Chen, *Angew. Chem. Int. Ed.*, 2014, **53**, 13488-13492.
24. L. Fransson, T. Eriksson, K. Edström, T. Gustafsson and J. O. Thomas, *J. Power Source.*, 2001, **101**, 1-9.
25. I. Kovalenko, B. Zdyrko, A. Magasinski, B. Hertzberg, Z. Milicev, R. Burtovyy, I. Luzinov and G. Yushin, *Science*, 2011, **334**, 75-79.
26. H. X. Ji, L. L. Zhang, M. T. Pettes, H. F. Li, S. S. Chen, L. Shi, R. Piner and R. S. Ruoff, *Nano Lett.*, 2012, **12**, 2446-2451.
27. H. Gwon, H.-S. Kim, K. U. Lee, D.-H. Seo, Y. C. Park, Y.-S. Lee, B. T. Ahn and K. Kang, *Energy Environ. Sci.*, 2011, **4**, 1277-1283.
28. Z. X. Huang, Y. Wang, Y. G. Zhu, Y. M. Shi, J. I. Wong and H. Y. Yang, *Nanoscale*, 2014, **6**, 9839-9845.
29. F. Liu, S. Y. Song, D. F. Xue and H. J. Zhang, *Adv. Mater.*, 2012, **24**, 1089-1094.
30. S. Y. Yin, Y. Y. Zhang, J. H. Kong, C. J. Zou, C. M. Li, X. H. Lu, J. Ma, F. Y. C. Boey and X. D. Chen, *ACS Nano*, 2011, **5**, 3831-3838.
31. M. Zhang, Y. Wang and M. Q. Jia, *Electrochim. Acta.*, 2014, **129**, 425-432.
32. L. Jiang and Z. Fan, *Nanoscale*, 2014, **6**, 1922-1945.
33. K. Rana, S. D. Kim and J.-H. Ahn, *Nanoscale*, 2015.
34. X. L. Li, H. L. Wang, J. T. Robinson, H. Sanchez, G. Diankov and H. J. Dai, *J. Am. Chem. Soc.*, 2009, **131**, 15939-15944.
35. Z.-S. Wu, W. Ren, L. Xu, F. Li and H.-M. Cheng, *ACS Nano*, 2011, **5**, 5463-5471.
36. L. L. Tian, X. Y. Wei, Q. C. Zhuang, C. H. Jiang, C. Wu, G. Y. Ma, X. Zhao, Z. M. Zong and S. G. Sun, *Nanoscale*, 2014, **6**, 6075-6083.
37. L. Y. Liang, Y. M. Xu, Y. Lei and H. M. Liu, *Nanoscale*, 2014, **6**, 3536-3539.
38. Z. S. Wu, W. C. Ren, L. Wen, L. B. Gao, J. P. Zhao, Z. P. Chen, G. M. Zhou, F. Li and H. M. Cheng, *ACS Nano*, 2010, **4**, 3187-3194.
39. L. Xiao, D. Q. Wu, S. Han, Y. S. Huang, S. Li, M. Z. He, F. Zhang and X. L. Feng, *ACS Appl. Mater. Interfaces*, 2013, **5**, 3764-3769.
40. Z.-S. Wu, W. Ren, L. Wen, L. Gao, J. Zhao, Z. Chen, G. Zhou, F. Li and H.-M. Cheng, *ACS Nano*, 2010, **4**, 3187-3194.
41. C. D. Wang, Y. G. Zhou, L. F. He, T. W. Ng, G. Hong, Q. H. Wu, F. Gao, C. S. Lee and W. J. Zhang, *Nanoscale*, 2013, **5**, 600-605.
42. Z. Jin, J. Yao, C. Kittrell and J. M. Tour, *ACS Nano.*, 2011, **5**, 4112-4117.
43. W. Y. Li, L. N. Xu and J. Chen, *Adv. Funct. Mater.*, 2005, **15**, 851-857.
44. R. H. Wang, C. H. Xu, M. Du, J. Sun, L. Gao, P. Zhang, H. L. Yao and C. C. Lin, *Small*, 2014, **10**, 2260-2269.
45. J. X. Zhu, T. Zhu, X. Z. Zhou, Y. Y. Zhang, X. W. Lou, X. D. Chen, H. Zhang, H. H. Hng and Q. Y. Yan, *Nanoscale*, 2011, **3**, 1084-1089.

Reprocessable Squeezing Electrode Fabrication of Olive-Like Fe/Co/O Nanoparticles@Three Dimensional Nitrogen-doped Reduced Graphene Oxide for High Performance Lithium Battery

Li-Ya Qi,[a] Yi-Wei Zhang,[a] Yue-Long Xin,[a] Zi-Cheng Zuo,[b]
Bin Wu,[b*] Xin-Xiang Zhang[a] and Heng-Hui Zhou[a*]

[a] College of Chemistry and Molecular Engineering, Peking University, Beijing, P. R. China.

[b] Beijing Engineering Research Center of Power Lithium-ion Battery, Beijing 102200

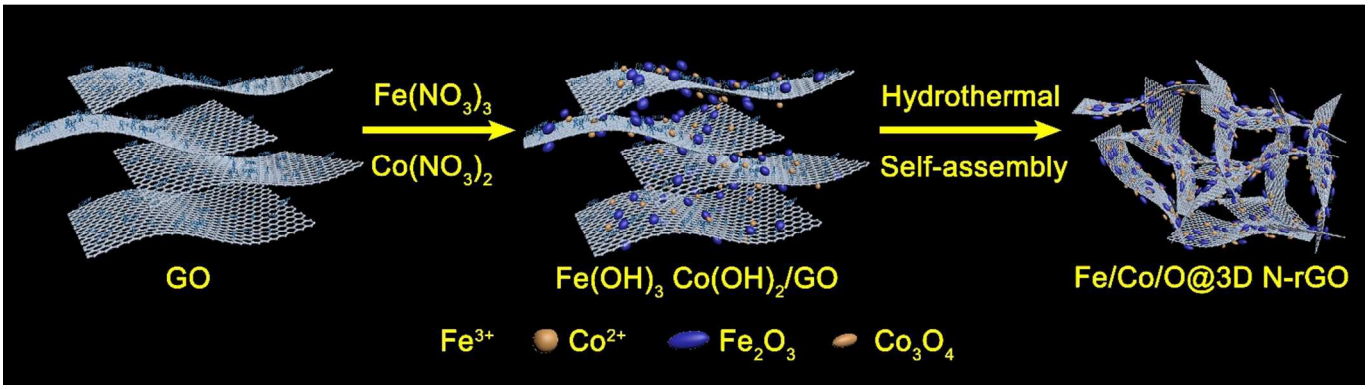

Figure 1 Schematic illustration of the synthesis process and structure of Fe/Co/O@3D N-rGO.

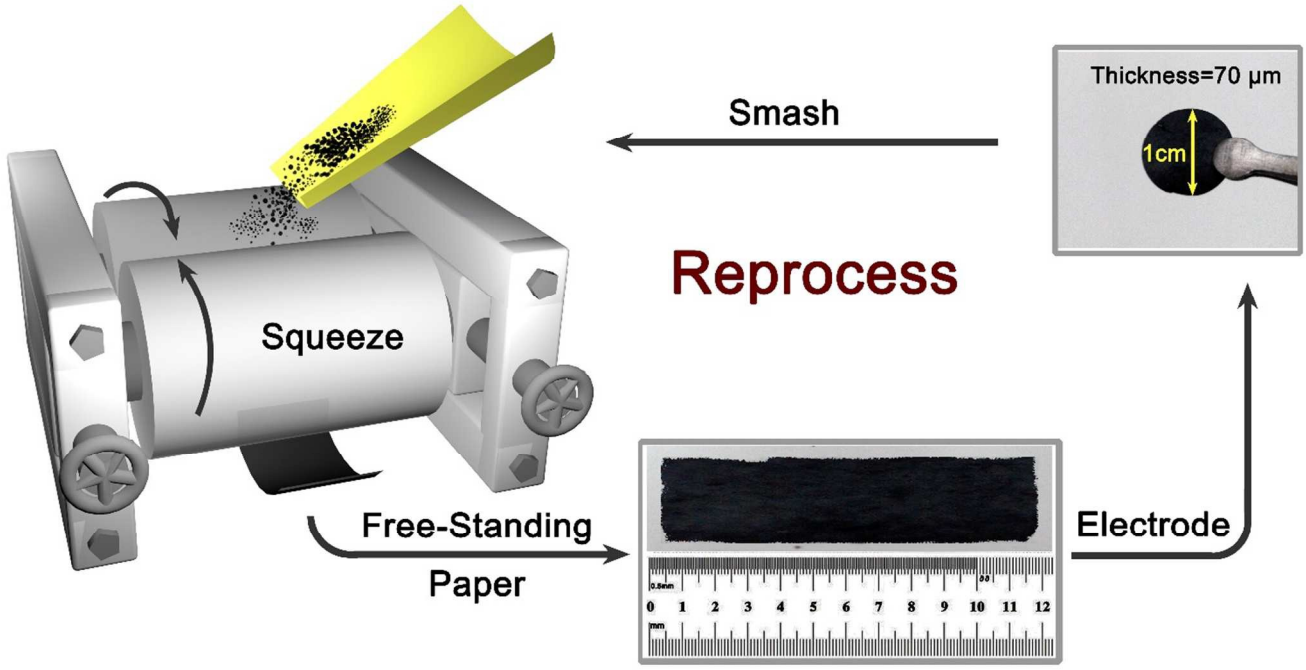

Figure 2 Schematic illustration of synthesis of free-standing electrodes through "squeezing" method and the related reprocessable process.

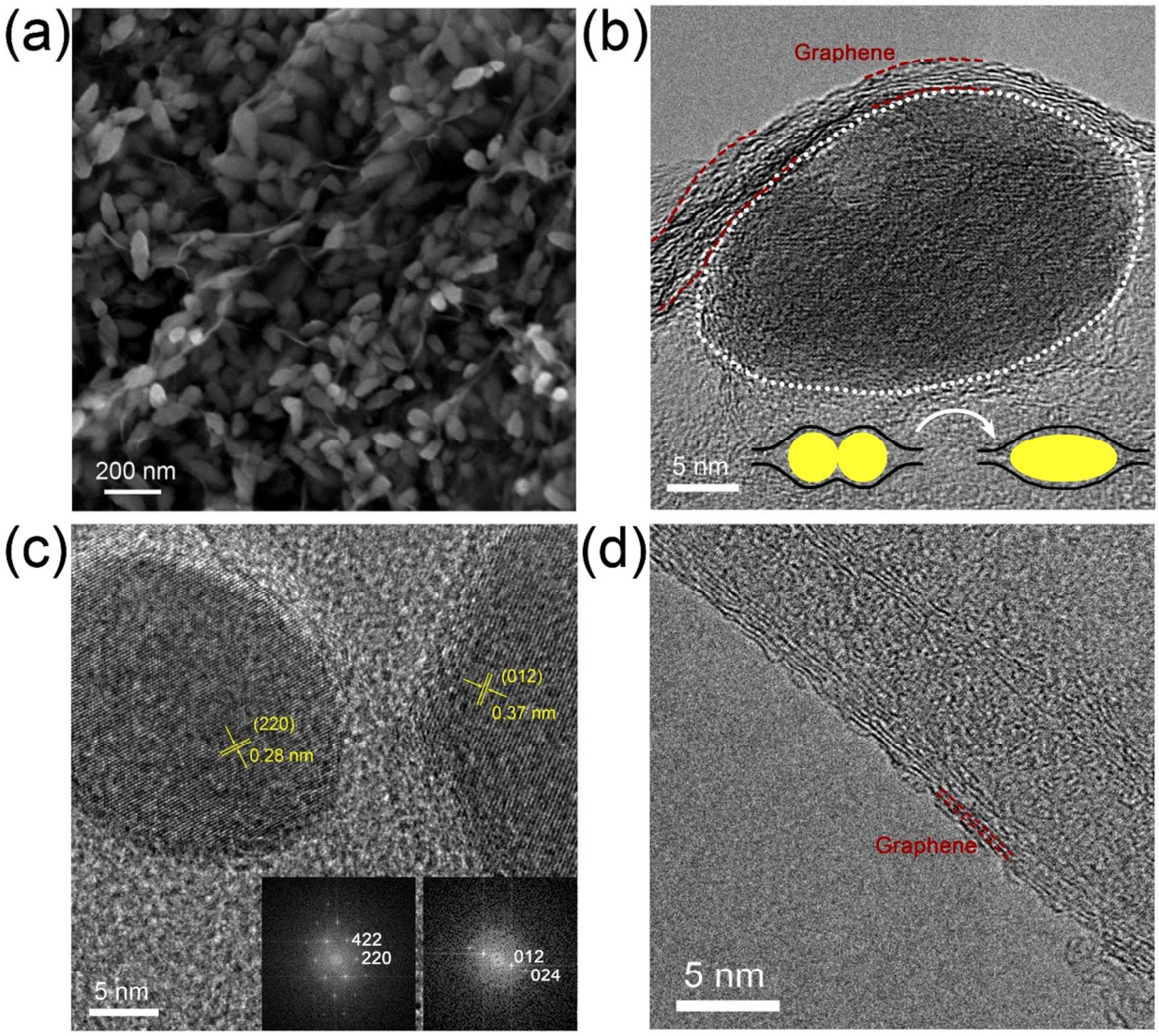

Figure 3 (a) SEM image of uniform distribution of Fe/Co/O particles. (b) HRTEM image of olive-like nanoparticles exited between graphene layers and their schematic description. (c) HRTEM image of the composite. (d) HRTEM image of folded edges of graphene.

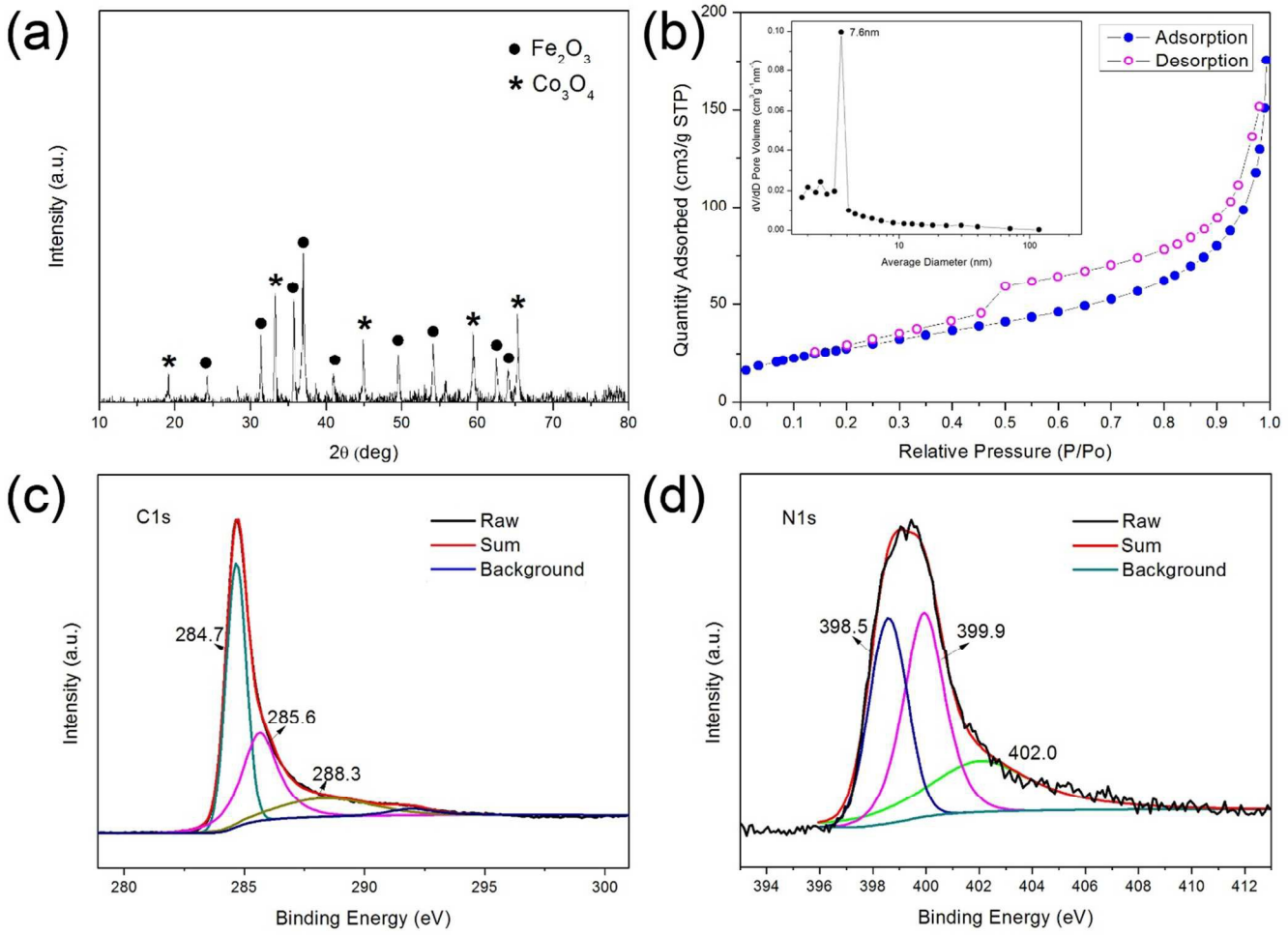

Figure 4 (a) XRD patterns of the obtained Fe/Co/O@3D N-rGO composite. (b) Nitrogen adsorption/desorption isotherms and pore size distribution of Fe/Co/O@3D N-rGO. (c) XPS C1s spectrum (d) N1s spectrum for Fe/Co/O@3D N-rGO.

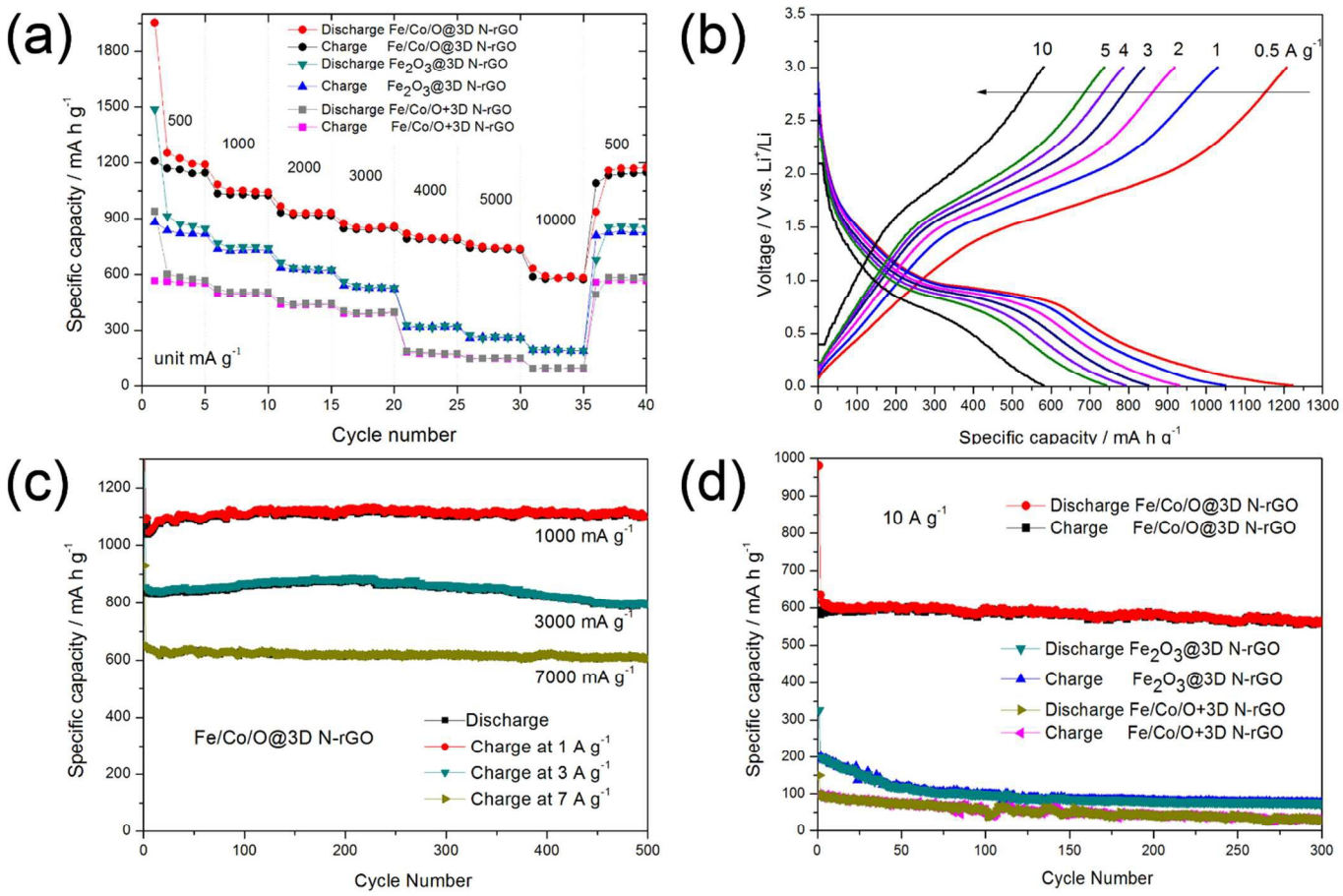

Figure 5 Electrochemical characterizations (a) Rate capacity of Fe/Co/O@3D N-rGO at different current densities. (b) The corresponding charge/discharge curves at various current densities (500-10000 mA g^{-1}). (c) Cycle performance at different current densities. (d) Comparative cycle performances of Fe/Co/O@3D N-rGO, Fe_2O_3@3D N-rGO and Fe/Co/O+3D N-rGO at a current density of 10A g^{-1}.

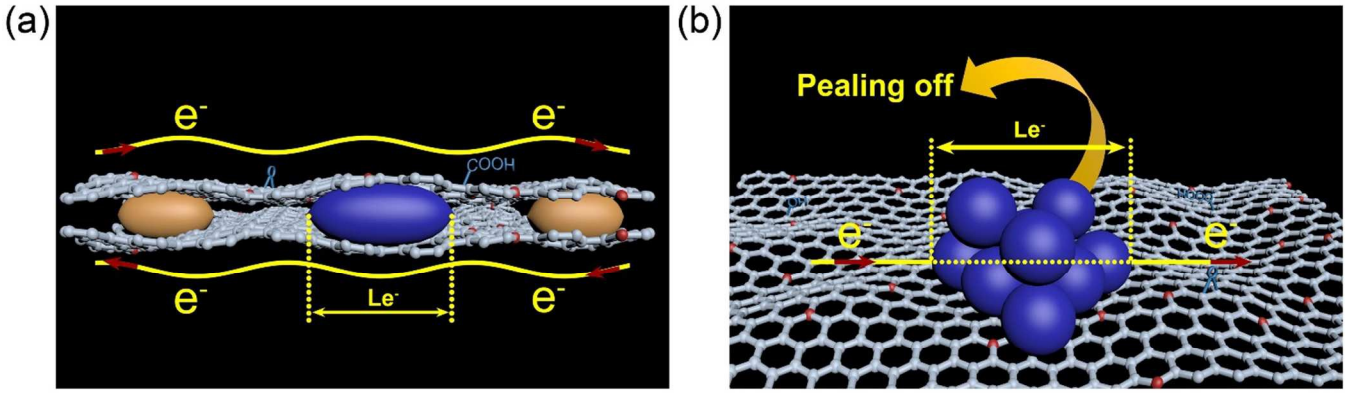

Figure 6 Schematic explanation of morphology changes during cycles and shows the comparative paths for lithium-ions and electrons (*Le*) for Fe/Co/O@3D N-rGO (a) and Fe/Co/O+3D N-rGO (b), respectively.